Nonlinear Dyn (2023) 111:12625–12638
https://doi.org/10.1007/s11071-023-08500-z

ORIGINAL PAPER

A modeling approach shows the effects of different light–dark schemes on the entrainment ability of the suprachiasmatic nucleus

Wenxin Zheng · Changgui Gu · Huijie Yang · Jos H. T. Rohling

Received: 14 November 2022 / Accepted: 13 April 2023 / Published online: 26 April 2023

Abstract In mammals, an endogenous clock located in the suprachiasmatic nucleus (SCN), synchronizes physiological and biological rhythms to the environmental light–dark cycle. In experiments, most researchers applied rectangular scheme as the external light–dark scheme received by the SCN neuronal oscillators. However, the external light intensity changes gradually throughout the day. Therefore, trapezoidal schemes (twilight) or sinusoidal schemes were also applied. Thus far, the effects of different light–dark schemes on the oscillators of the SCN did not get fully explored. In the present study, we theoretically analyzed how the five common light–dark schemes affect the entrainment ability of the SCN, based on a Poincaré model. We numerically found that when the maximum light intensity, the minimum light intensity, and the total amount of light exposure per cycle were the same, the largest entrainment range was obtained in the oscillators receiving more light in the daytime. However if, under the condition of 12:12-h illumination, the total amount of light exposure per cycle was the same, the maximum light intensity during the day leaded to an increased range of entrainment. Moreover, the entrainment range was reduced when the photoperiod was extended. Note that, increasing the maximum light intensity increased the entrainment ability of all light–dark schemes. Our results exposes the important role of light–dark schemes in the entrainment ability of the SCN network, and provides a potential explanation for the diversity of the entrainment range between diurnal and nocturnal animals.

Keywords SCN neuronal network · Circadian rhythms · Light–dark schemes · Entrainment range · Mathematical modeling

1 Introduction

Due to the rotation of the Earth, the period of the light–dark cycle is fixed at 24 h, while the intensity of environmental light changes gradually throughout the day [1]. Under natural conditions, the intensity and the duration of light vary with geographical latitudes and local seasons [1]. For example, although the daily insolation values at the equator and the arctic pole are similar at summer solstice, the intensity of light is higher and the duration is shorter at the equator, while the intensity of light is lower and the duration is longer in the arctic pole [1]. In most typical laboratory conditions for circadian rhythm research, a rectangular scheme of light–dark alternation was often applied [2–4]. In experimental

Supplementary Information The online version contains supplementary material available at https://doi.org/10.1007/s11071-023-08500-z.

W. Zheng · C. Gu (✉) · H. Yang
Business School, University of Shanghai for Science and Technology, Shanghai 200093, China
e-mail: Gu_changgui@163.com

J. H. T. Rohling
Department of Cell and Chemical Biology, Leiden University Medical Center, 2300RC Leiden, The Netherlands

studies, it has been shown that the light–dark scheme affects the circadian rhythm.

The circadian rhythm of organisms is entrained by the environmental light–dark cycle [5]. When the daily photoperiod changes, the organism will entrain to the corresponding period [3,6]. For example, a Eutamias sibiricus can be entrained between 14.9 h (the lower limit of entrainment, LLE) and 32.4 h (the upper limit of entrainment, ULE), a human being can be entrained between 20.5 h and 29 h, and a Microcebus murinus can be entrained between 21.2 h and 25.3 h [3,6–8]. The range that the organism can be entrained from the LLE to the ULE is called the entrainment range [3,9]. The entrainment range is a collective behavior of the organism and reflects the flexibility of the organism to entrain to the external light–dark cycle.

In mammals, the entrainment is ensured by an endogenous biological clock, which is located in the suprachiasmatic nucleus (SCN) of the brain [10–14]. The SCN is located in the anterior hypothalamus and composed of about 20,000 heterogeneous neuronal oscillators [6,15]. These neuronal oscillators oscillate autonomously with nonidentical periods and form a network through neurotransmitter coupling [7,16–19]. According to the neurotransmitters released by these neuronal oscillators and the sensitivity to the light information, the SCN can be divided into two different subgroups, one is the ventrolateral (VL) subgroup located in the core of the SCN, and the other is the dorsomedial (DM) subgroup surrounding the core [20]. The VL subgroup contains neuronal oscillators that are directly sensitive to the light information, and transmit this light information to the light-insensitive neuronal oscillators located in the DM subgroup through the release of neurotransmitter vasoactive intestinal peptide (VIP) [20–22]. The DM subgroup converts the rhythmic VIP signal into circadian oscillation of the neurotransmitter arginine vasopressin (AVP), resulting in uniform and robust circadian rhythms [20,23].

The flexibility and robustness of the SCN to respond quickly to changes in the external environment are vitally important for its proper function. Light is the most potent and important Zeitgeber (i.e., the time giver) for organisms to become synchronized with the 24 h rhythm on earth, and has a great impact on the SCN [24,25]. Understanding the light entrainment of the circadian rhythm in the SCN is very important. When the SCN is exposed to irregular light signals, it may result in numerous pathologies [4].

Under laboratory conditions, in order to facilitate the control of lighting conditions, rectangular schemes were often applied [2–4]. However, the light intensity in the environment changes gradually throughout the day [3]. Schmal et al. assumed that the natural light conditions vary sinusoidally [1]. A number of other experimental studies considered twilight schemes as being closer to natural light conditions. Twilight schemes are trapezoidal schemes, which are basically rectangular schemes with a one or two-hour linear transition between light and darkness and between darkness and light [26–29]. As far as we know, the effects of different light–dark schemes on the oscillators of the SCN did not get fully explored. The present study considered a rectangular scheme, a trapezoidal scheme, and a sinusoidal scheme, but also considered two other light–dark schemes, triangular and sawtooth.

Experimental studies compared either a sinusoidal or a twilight scheme to a rectangular scheme showed that the rectangular scheme led to a smaller range of entrainment [3,26,27]. Comas, et al., explored the differences of the twilight conditions in different photoperiods and the 12-12 h rectangular scheme (equinox) [29]. They looked for 1-hour and 2-hour twilight conditions, and the results were not consistent with the findings of Boulos, et al [28]. Therefore, We analyzed how the maximum light intensity during the day and the total amount of light exposure during the day influenced the entrainment ability of the SCN, and we examined the influences of different photoperiods on the entrainment ability of the SCN.

In the present study, we examined the effects of different light–dark schemes received by the SCN neuronal oscillators on the entrainment range, based on a Poincaré model [6,30–32]. The rest of this paper is organized as follows. In Sect. 2, several light–dark schemes are described, and a Poincaré model is introduced to describe the SCN neuronal network exposed to the external light–darkness cycle. Then, in Sect. 3, the effects of different light–dark schemes received by the SCN neuronal oscillators on the entrainment range are compared by numerical simulations. After that, in Sect. 4, the theoretical explanations are given to confirm the simulation results in Sect. 3. Finally, conclusions are drawn and discussions are presented in Sect. 5.

2 Methods

2.1 Description of the light–dark schemes

In this section, we introduced the five common cyclic schemes representing the alternation of light and dark in Fig. 1. For simplicity, the LD, the TRA, the SINE, the TRI and the SAW represent the rectangular scheme, the trapezoidal scheme, the sinusoidal scheme, the triangular scheme, and the sawtooth scheme, respectively. Note that 0–12 h corresponds to the daytime and 12–24 h corresponds to the nighttime with in one 24 h cycle. In order to ensure that the maximum light intensity, the minimum light intensity, and the total amount of light exposure per cycle were consistent, the rectangular scheme was the only scheme that received light only during the day-time, and the other schemes also received light during the night, resulting in less light during the day-time.

Most of the literatures, especially in laboratory conditions, introduced the rectangular scheme, and a few introduced the sinusoidal scheme [1,3]. Therefore, we performed additional tests on the rectangular and sinusoidal schemes in order to draw more general conclusions. As the photoperiod, the light intensity and the total amount of light exposure in one cycle affect the entrainment range, we considered the rectangular scheme and several common sinusoidal schemes in Fig. 2, where (a) and (d) correspond to Fig. 1(a) and (b), respectively. Note that we only considered the 12:12 h rectangular scheme. The sinusoidal schemes of (b) and (c) both received 12 h illumination only at the day-time. Among them, the total amount of light exposure in one cycle were the same in (a), (b), and (d),

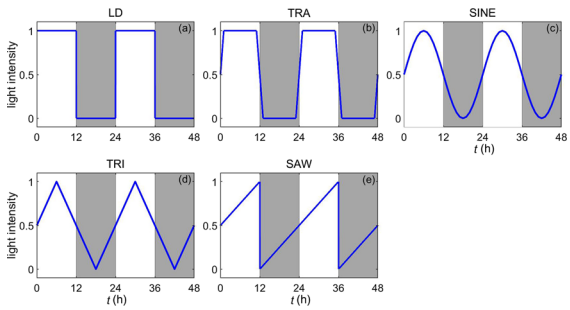

Fig. 1 (Color online). Scheme of the five schemes for light and darkness in one 24-h cycle. Note that white background corresponds to the daytime and gray background corresponds to the nighttime

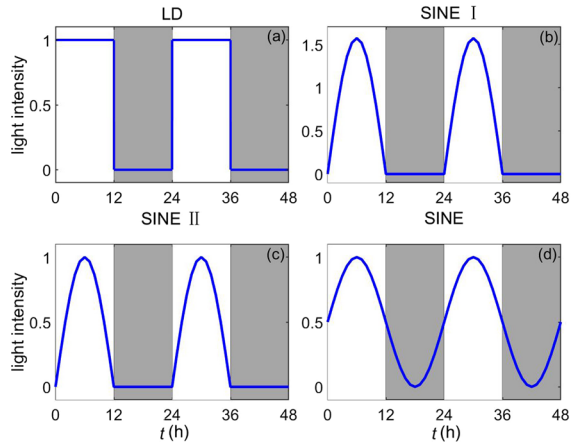

Fig. 2 (Color online). Scheme of the 12:12 h rectangular scheme and different sinusoidal schemes when exposed to the external light–dark cycle for 24 h. Note that white background corresponds to the daytime and gray background corresponds to the nighttime

while the maximum light intensity of (a), (c), and (d) were the same.

The total amount of light exposure and the photoperiod in one cycle have an important influence on the entrainmentg ability of the SCN neuronal oscillators. The present studies took the rectangular scheme and the sinusoidal scheme as examples to conduct in-depth research in Figs. 3 and 4, respectively. When the photoperiod was expanded, the total amount of light exposure can maintain constantly by reducing the maximum light intensity. Conversely, when the photoperiod was shortened, the total amount of light exposure can maintain constantly by increasing the maximum light intensity. In Fig. 3(a) and (c) were 12 h light–dark schemes, i.e., the SCN neuronal oscillators only 0–12 h received light in one 24-h cycle. (b) and (d) were 16 h light–dark schemes, i.e., the SCN neuronal oscillators only 0–16 h received light in one 24-h cycle. In (c), the total amount of light exposure in one 24-h cycle was the same as in (b). This leaded to a higher maximum light intensity during midday. In (d), the total amount of light exposure in one 24-h cycle was the same as in (a). This leaded to a lower maximum light intensity during midday. Fig. 4 was similar to Fig. 3.

2.2 Description of the Poincaré model

In the field of circadian rhythm, there are mainly two types of models used to describe the oscillatory behav-

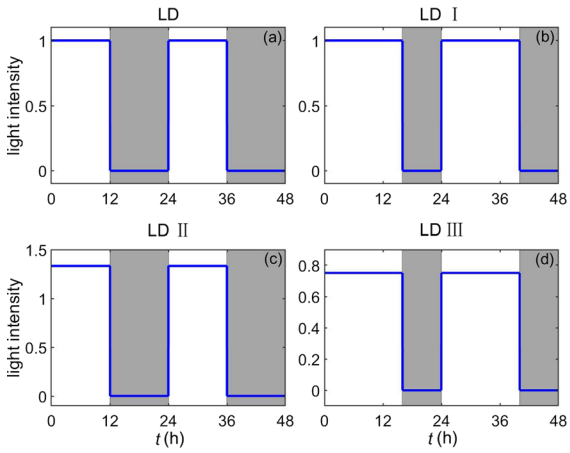

Fig. 3 (Color online). Rectangular light–dark schemes of 24-h cycles. (**a**) and (**c**) correspond to 12-h photoperiod, and (**b**) and (**d**) correspond to 16-h photoperiod. Note that, the total amount of light exposure in (**a**) and (**d**) are the same, and the total amount of light exposure in (**b**) and (**c**) are the same

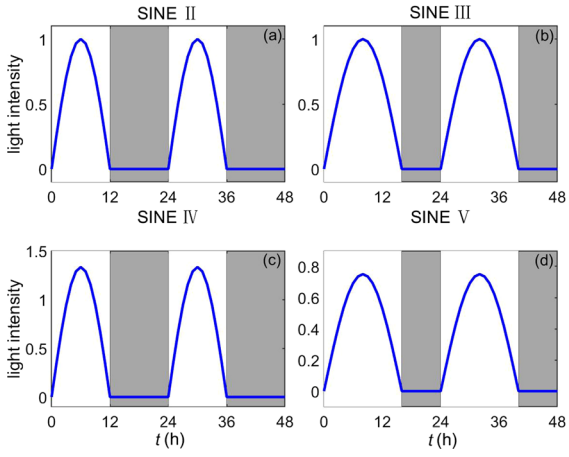

Fig. 4 (Color online). Sinusoidal light–dark schemes of 24-h cycles. (**a**) and (**c**) correspond to 12-h photoperiod, and (**b**) and (**d**) correspond to 16-h photoperiod. Note that, the total amount of light exposure in (**a**) and (**d**) are the same, and the total amount of light exposure in (**b**) and (**c**) are the same

ior of the SCN neuronal oscillators, i.e., the biophysical models (such as the Goodwin model) and the general models (such as the Poincaré model and the Kuramoto model) [6,32,33]. The Goodwin model describes the neuronal oscillator through a genetic feedback loop, the Kuramoto model is purely based on the phase of the oscillator, while the Poincaré model is an abstract model, which uses a more general description of the oscillator. Here the Poincaré model was chosen for numerical simulation, because of its generality and more direct theoretical analysis method.

In the present study, the Poincaré model was introduced to simulate the SCN network composed of N neuronal oscillators [34–38]. Each neuronal oscillator is represented by two variables x and y [6,30,32,39]. The subscript i represents the i_{th} neuronal oscillator, and its dynamics are described as follows

$$\begin{aligned}
\dot{x}_i &= \gamma x_i(A - r_i) - \frac{2y_i\pi}{\tau} + gF + K_f L_i, \\
\dot{y}_i &= \gamma y_i(A - r_i) + \frac{2x_i\pi}{\tau}, \\
F &= \frac{1}{N}\sum_{i=1}^{N} x_i, \quad i = 1, 2, \cdots, N,
\end{aligned} \tag{1}$$

where the parameters γ, A, τ, g and N represent the amplitude relaxation rate, intrinsic amplitude, intrinsic period, coupling strength and the total number of neuronal oscillators, respectively. For simplicity, the SCN was assumed to be an all-to-all connected network, i.e., all the neuronal oscillators were coupled under the function of the mean field F representing neurotransmitters, where the value of F depended on the average value of the output variable x of all the neuronal oscillators. The parameter r_i is the coupling amplitude of the i_{th} neuronal oscillator, which is defined as

$$r_i = \sqrt{x_i^2 + y_i^2}. \tag{2}$$

$K_f L_i$ represents the external light input to the neuronal oscillator i, where K_f is the light-sensitivity. The value of parameter K_f is different in different subgroups. In this paper, we assumed that the VL subgroup contains 50% SCN neuronal oscillators and the DM subgroup composed of the rest 50% SCN neuronal oscillators. If the neuronal oscillator i was located in the VL subgroup, the parameter $K_f \neq 0$; if the neuronal oscillator i was located in the DM subgroup, whether during the daytime or the nighttime, the parameter $K_f = 0$. In this study, the key parameter L_i depended on the light–dark scheme received by the neuronal oscillators exposed to the light–dark cycle with external period T. A rectangular scheme can be described as follows

$$L_i = \begin{cases} 1, & mod(t, T) \le \dfrac{T}{2}, \\ 0, & mod(t, T) > \dfrac{T}{2}. \end{cases} \tag{3}$$

A trapezoidal scheme can be described as follows

$$L_i = \begin{cases} \frac{12}{T} mod(t,T) + \frac{1}{2}, & mod(t,T) \le \frac{T}{24}, \\ 1, & \frac{T}{24} < mod(t,T) \le \frac{11T}{24}, \\ \frac{13}{2} - \frac{12}{T} mod(t,T), & \frac{11T}{24} < mod(t,T) \le \frac{13T}{24}, \\ 0, & \frac{13T}{24} < mod(t,T) \le \frac{23T}{24}, \\ \frac{12}{T} mod(t,T) - \frac{23}{2}, & mod(t,T) > \frac{23T}{24}. \end{cases} \tag{4}$$

A sinusoidal scheme can be described as follows

$$L_i = \frac{\sin(\frac{2\pi}{T}t) + 1}{2}. \tag{5}$$

A triangular scheme can be described as follows

$$L_i = \begin{cases} \frac{2}{T} mod(t,T) + \frac{1}{2}, & mod(t,T) \le \frac{T}{4}, \\ \frac{3}{2} - \frac{2}{T} mod(t,T), & \frac{T}{4} < mod(t,T) \le \frac{3T}{4}, \\ \frac{2}{T} mod(t,T) - \frac{3}{2}, & mod(t,T) > \frac{3T}{4}. \end{cases} \tag{6}$$

A sawtooth schemet can be described as follows

$$L_i = \begin{cases} \frac{1}{T} mod(t,T) + \frac{1}{2}, & mod(t,T) \le \frac{T}{2}, \\ \frac{1}{T} mod(t,T) - \frac{1}{2}, & mod(t,T) > \frac{T}{2}, \end{cases} \tag{7}$$

where the parameter t is the external time. For the photoperiod studies, where the photoperiod was changed, the light–dark schemes have been modified accordingly, and were adjusted for the prolonged photoperiod. For example, the rectangular scheme for 16 h light and 8 h darkness is as follows

$$L_i = \begin{cases} 1, & mod(t,T) \le \frac{2T}{3}, \\ 0, & mod(t,T) > \frac{2T}{3}. \end{cases} \tag{8}$$

2.3 Definition of the LLE

In Sect. 3, we will study the effects of different light–dark schemes on the entrainment range of the SCN. Here, the lower limit of entrainment (LLE) was used to represent the entrainment range [6]. The smaller the LLE was, the larger the entrainment range was, and vice versa. If the difference between the period T_i of the i_{th} neuronal oscillator and the external light–dark period T was less than 0.00001 h, the SCN was considered to be entrained by the external light–dark cycle [6]. The value of T_i was calculated according to the evolution of variable y_i.

Since the free running period of the SCN was affected by the coupling strength g, we standardized the LLE as follows

$$\mathrm{LLE}_{\mathrm{normalized}} = \frac{\mathrm{LLE}}{\mathrm{FRP(g)}} \times 24, \tag{9}$$

where FRP(g) represents the free running period of the neuronal oscillators when the coupling strength is g. For simplicity, we used the LLE to represent the $\mathrm{LLE}_{\mathrm{normalized}}$ in this paper.

2.4 Simulation details

In the numerical simulation, we set the parameters as $\gamma = 0.03$, $A = 1$ and $\tau = 24$ [6]. The value of g was selected between 0 and 0.2. At present, no researches have found whether the light sensitivity was larger than the coupling strength, so the four light sensitivities considered here were $K_f = 0.05, 0.10, 0.15$ and 0.20. Without special instructions, the number of neuronal oscillators N was 2, i.e., each subgroup contains 1 neuronal oscillator.

The fourth-order Runge–Kutta method was introduced for the numerical simulation, in which the time step was 0.01 h. To avoid the effect of transients, we ignored the initial 1,000,000 time steps (10,000 h). In this model, the initial conditions for the variables x_i and y_i were randomly selected from a uniform distribution of 0 to 1.

3 Simulation results

Figure 5 shows non-entrained and entrained conditions of the SCN model. In (a), the external period is 22 h, and both the VL and the DM subgroups are not able to entrain to this external condition, because the periods of both subgroups can not synchronize to the external period of light and darkness. (b) shows an entrained condition, as both subgroups adhere to the 24 h external light–dark cycle, and as such the external cycle entrains both subgroups to a 24 h period. To find the range of entrainment for the SCN model, we look for the lowest external period to which the system entrains. This is called the lower limit of entrainment (LLE).

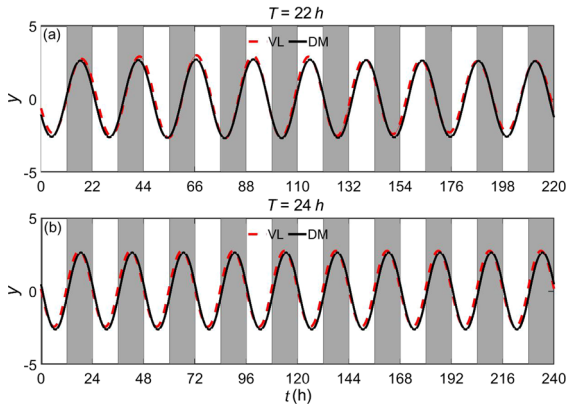

Fig. 5 (Color online). The temporal evolution of neuronal oscillators in the VL and the DM subgroups exposed to the sinusoidal scheme cycles of 22 h and 24 h, respectively. The y-axis represents the amplitude of each subgroup of the SCN. Gray background corresponds to darkness and white background corresponds to light. The coupling strength g and the light sensitivity K_f are both equal to 0.10

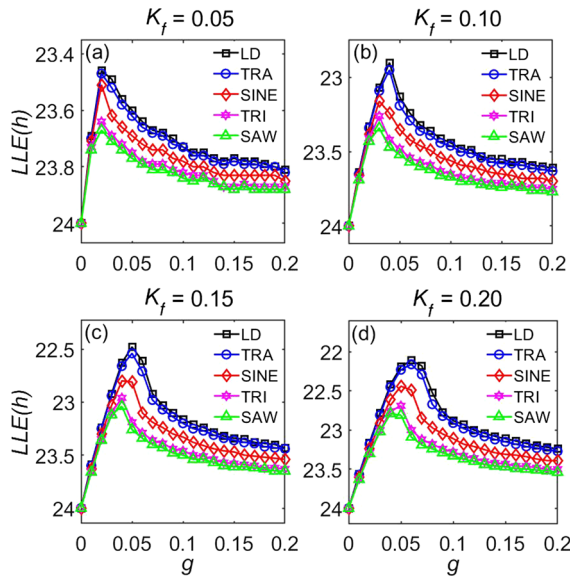

Fig. 6 (Color online). The comparison in the relationship of the LLE to the coupling strength g among the five light–dark schemes in Fig. 1. The four light sensitivity values K_f = 0.05, 0.10, 0.15 and 0.20 are considered in (**a**)–(**d**)

3.1 Compare the five light–dark schemes

For each of the different light–dark schemes shown in Fig. 1, the LLE is calculated in Fig. 6. In (a), the relationship between the LLE and the coupling strength g for the different schemes are showed, when the light intensity K_f = 0.05. These are calculated for different values of the coupling strength between all neuronal oscillators. For the five light–dark schemes considered in this section, we observe that there is a similar parabolic relationship between the LLE and g, which is comparable to what was found in Ref. [32]. With the increase of coupling strength g, the LLE decreases first and then increases, i.e., the range of entrainment becomes larger first and then becomes smaller. When the coupling strength g reaches a certain critical value g_c, the maximum entrainment range is obtained. When the coupling strength g = 0, i.e., there is no coupling between the neuronal oscillators, the LLE of all light–dark schemes are the same as the intrinsic period τ of the individual oscillator.

The order of the different light–dark schemes going from the largest entrainment range to the smallest is rectangular scheme, trapezoidal scheme, sinusoidal scheme, triangular scheme and sawtooth scheme. When the maximum entrainment range is obtained, i.e., near the critical value g_c, the discrimination of the influences for the five light–dark schemes on the entrainment range is the largest.

To examine if the light sensitivity K_f affects the entrainment range, different light sensitivity values K_f = 0.10, 0.15 and 0.20 are examined in Fig. 6(b)–(d). The results show that the parabolic nature has not changed and the order of the different light–dark schemes is also the same. The only difference that can be noted is that a higher light sensitivity leads to a larger (maximum) entrainment range.

Through comparing the five light–dark schemes, we find that when the maximum light intensity, the minimum light intensity, and the total amount of light exposure per cycle are the same, the neuronal oscillators that receive more light in the day-time obtain a larger entrainment range. In addition, with the increase of the light sensitivity, i.e., exposure, the entrainment range of the five light–dark schemes increases, but their order is not affected.

Next, we study the influence of the number of the SCN neuronal oscillators on the entrainment range of the five different light–dark schemes. We select the number of neuronal oscillators to be N = 200 for the numerical simulation, i.e., each subgroup contains 100 neuronal oscillators. The results shown in Fig. 7 are comparable to those shown in Fig. 6. Thus, the number of neuronal oscillators does not affect the influence of the light–dark scheme on the entrainment range.

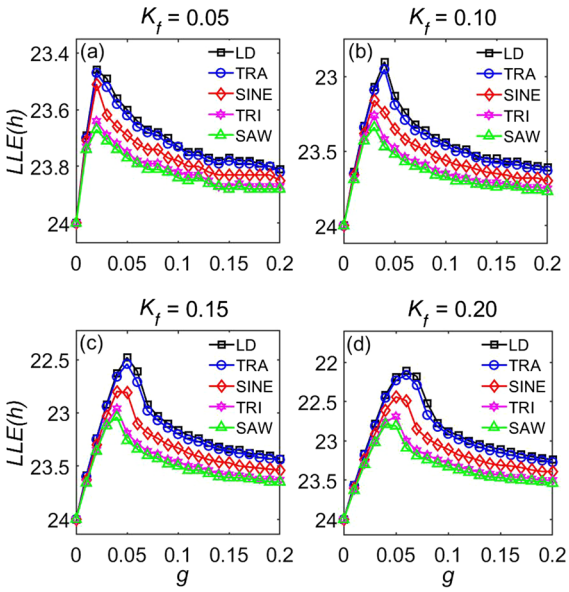

Fig. 7 (Color online). The comparison in the relationship of the LLE to the coupling strength g among the five light–dark schemes when the number of oscillators of the SCN are N = 200. Other parameter values are the same as those in Fig. 6

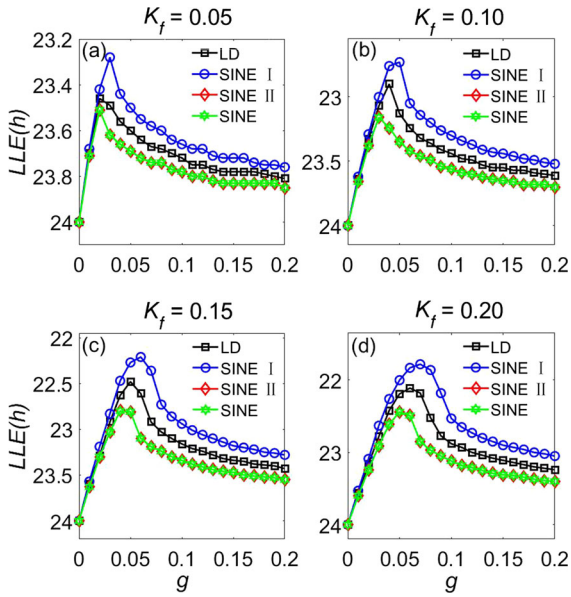

Fig. 8 (Color online). The comparison in the relationship of the LLE to the coupling strength g among the 12:12 h rectangular scheme and several different sinusoidal schemes shown in Fig. 2. Other parameter values are the same as those in Fig. 6

3.2 Compare the 12:12 h rectangular scheme with several different sinusoidal schemes

In Figs. 6 and 7, we have seen that the rectangular scheme leads to the highest entrainment range, and this coincides with the fact that all light in this condition is given during the day, and not during the night. All the other light–dark schemes also have partial illumination during the night period, and as the total amount of light exposure is the same for all schemes, the amount of light exposure during the day is smaller in those other light–dark schemes. To investigate the influences of light during the day more closely, we have designed a number of variants from the sinusoidal schemes in Fig. 2. The results of the simulations are shown in Fig. 8.

The total amount of light exposure in one 24-h cycle of SINE I is the same as LD, which leads to a higher maximum light intensity during midday. The maximum light intensity of SINE II is the same as LD. This leads to a lower total amount of light exposure in one cycle. SINE I leads to a larger entrainment range compared to the LD, while for SINE II, the entrainment range is smaller than the LD. SINE II has the exact same entrainment range as SINE. As total amount of light exposure in one 24-h cycle are the same for both schemes, this indicates that light during the night does not affect the entrainment range. Only light during the day changes the range of entrainment. Therefore, more light during the day and higher maximum light intensity both positively affect the entrainment range of the SCN.

3.3 Compare the four rectangular schemes

We now investigate if prologing the day-time, simulating seasonal summer time, affects the range of entrainment. The simulation results of the four rectangular schemes are shown in Fig. 9. Comparing LD and LD II (or LD I and LD III), it can be found that when the photoperiod is the same, the entrainment range increases with the increase of the maximum light intensity, which is consistent with the result in Fig. 8. Comparing LD and LD I, when the maximum light intensity is the same and the photoperiod is extended from 12 h to 16 h, the entrainment range decreases, which means that increasing the photoperiod will decrease the entrainment range.

It is not difficult to verify that the entrainment range of LD II is larger than that of LD I, and the entrainment range of LD is larger than that of LD III, because

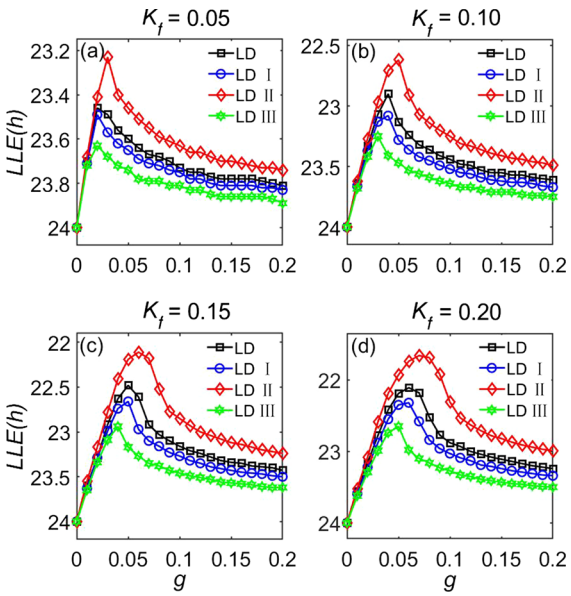

Fig. 9 (Color online). The comparison in the relationship of the LLE to the coupling strength g among the rectangular schemes shown in Fig. 3. The four light sensitivity values $K_f = 0.05, 0.10, 0.15$ and 0.20 are considered in (**a**)–(**d**)

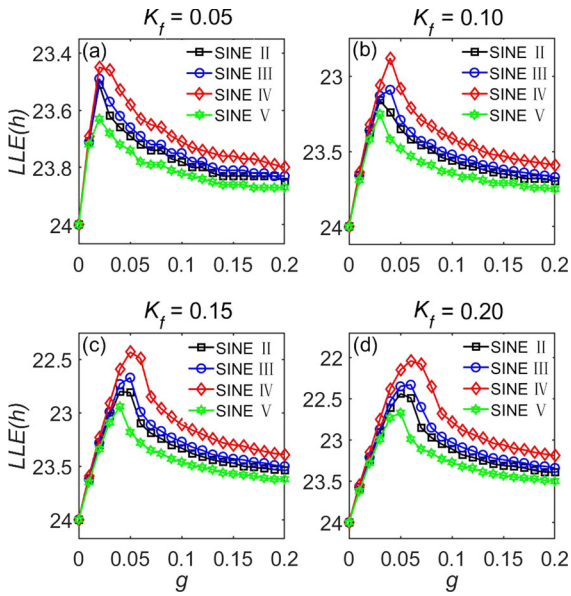

Fig. 10 (Color online). The comparison in the relationship of the LLE to the coupling strength g among the sinusoidal schemes shown in Fig. 4. The four light sensitivity values $K_f = 0.05, 0.10, 0.15$ and 0.20 are considered in (**a**)–(**d**)

when the total amount of light exposure is the same, the entrainment range will be reduced by prolonging the photoperiod and decreasing the maximum light intensity.

3.4 Compare the four sinusoidal schemes

We also investigate the prolonged day-time in sinusoidal schemes, where we take the half-sinusoidal scheme of SINE II as a basis. The simulation results of the four sinusoidal schemes are shown in Fig. 10. Comparing SINE II and SINE IV (or SINE III and SINE V), when the photoperiod is the same, the entrainment range increases with the increase of the maximum light intensity. The results show that the entrainment range of SINE IV is larger than that of SINE III, and the entrainment range of SINE II is larger than that of SINE V, which is consistent with the simulation results of the rectangular scheme shown in Fig. 9. When the total amount of light exposure is the same, the entrainment range is still increased when the photoperiod is shortened and the maximum light intensity is increased. Comparing SINE II and SINE III, when the maximum light intensity is the same and the photoperiod is extended from 12 h to 16 h, the entrainment range increases, which is inconsistent with the results of the rectangular scheme.

3.5 Compare the different photoperiods of the rectangular scheme and the sinusoidal scheme

To investigate why the photoperiod extension from 12 h to 16 h gives different results of the rectangular scheme and the sinusoidal scheme, we systematically study the relationship between the LLE and the photoperiod of these two schemes in Fig. 11. The simulation results show that with the increase of the photoperiod from 0 h to 24 h, the entrainment range of the rectangular scheme and the sinusoidal scheme increases first and then decreases. Note that, the rectangular scheme obtains the maximum entrainment range at a photoperiod of 12 h, while the sinusoidal scheme obtains the maximum entrainment range at 16 h. Our research find that different photoperiods change the entrainment ability of the SCN.

4 Theoretical analysis

The numerical simulation results in Sect. 3 showed that the number of neuronal oscillators did not affect the final results. In order to facilitate the theoretical

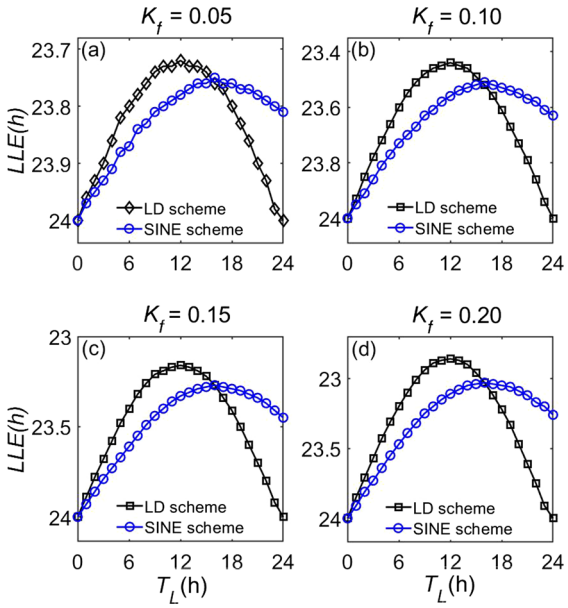

Fig. 11 (Color online). The comparison in the relationship of the maximum LLE to the different photoperiods among the rectangular scheme and the sinusoidal scheme. The x-axis shows the number of hours of light in the 24-h cycle. The four light sensitivity values K_f = 0.05, 0.10, 0.15 and 0.20 are considered in (**a**)–(**d**)

analysis, we consider the case of two neuronal oscillators, i.e., one neuronal oscillator a represents the VL and the other neuronal oscillator b represents the DM. Therefore, the Poincaré model can be simplified as follows

$$\begin{aligned}
\dot{x}_a &= \gamma x_a(A - r_a) - \omega y_a + g\frac{x_a + x_b}{2} + K_f L_i,\\
\dot{y}_a &= \gamma y_a(A - r_a) + \omega x_a,\\
\dot{x}_b &= \gamma x_b(A - r_b) - \omega y_b + g\frac{x_a + x_b}{2},\\
\dot{y}_b &= \gamma y_b(A - r_b) + \omega x_b,
\end{aligned} \tag{10}$$

where the intrinsic frequency ω is $\frac{2\pi}{\tau}$. For convenience, we convert Eq. (10) from Cartesian Coordinates to Polar Coordinates and introduce parameters θ_a and θ_b. let $x_a = r_a\cos\theta_a$, $y_a = r_a\sin\theta_a$, $x_b = r_b\cos\theta_b$, $y_b = r_b\sin\theta_b$, $\phi_a = \theta_a - \Omega t$, and $\phi_b = \theta_b - \Omega t$. Substituting them into Eq. (10), we obtain

$$\begin{aligned}
\dot{r}_a &= \gamma r_a(A - r_a) + \frac{g r_a}{2}\cos^2(\phi_a + \Omega t)\\
&\quad + \frac{g r_b}{2}\cos(\phi_b + \Omega t)\cos(\phi_a + \Omega t)\\
&\quad + K_f L_i\cos(\phi_a + \Omega t),\\
\dot{\phi}_a &= \omega - \frac{g}{2}\cos(\phi_a + \Omega t)\sin(\phi_a + \Omega t)\\
&\quad - \frac{g r_b}{2 r_a}\cos(\phi_b + \Omega t)\sin(\phi_a + \Omega t)\\
&\quad - \frac{K_f L_i}{r_a}\sin(\phi_a + \Omega t),\\
\dot{r}_b &= \gamma r_b(A - r_b) + \frac{g r_a}{2}\cos(\phi_a + \Omega t)\cos(\phi_b + \Omega t)\\
&\quad + \frac{g r_b}{2}\cos^2(\phi_b + \Omega t),\\
\dot{\phi}_b &= \omega - \frac{g r_a}{2 r_b}\cos(\phi_a + \Omega t)\sin(\phi_b + \Omega t)\\
&\quad - \frac{g}{2}\cos(\phi_b + \Omega t)\sin(\phi_b + \Omega t).
\end{aligned} \tag{11}$$

In order to simplify Eq. (11), the averaging method developed by Krylov and Bogoliubov in Refs. [6,30,32,40] is applied. As ϕ has a lower timescale than Ωt, the parameter $\alpha = <\phi_a> - <\phi_b>$ is introduced, where $<\cdot>$ represents the average value of a light–dark period. Equation (12) can be obtained by integration:

$$\begin{aligned}
&<\cos^2(\phi_a + \Omega t)> = \frac{1}{2},\\
&<\cos(\phi_b + \Omega t)\cos(\phi_a + \Omega t)> = \frac{\cos\alpha}{2},\\
&<\cos(\phi_a + \Omega t)\sin(\phi_a + \Omega t)> = 0,\\
&<\cos(\phi_b + \Omega t)\sin(\phi_a + \Omega t)> = \frac{\sin\alpha}{2}.
\end{aligned} \tag{12}$$

When all the neuronal oscillators in the SCN are entrained to the external light–dark cycle T, $\dot{r}_a = 0$, $\dot{r}_b = 0$, $\dot{\phi}_a = \Omega$ and $\dot{\phi}_b = \Omega$ can be obtained. Through substituting Eq. (12) into Eq. (11), the following simplified formula Eq. (13) can be obtained

$$\begin{aligned}
0 &= \gamma r_a(A - r_a) + \frac{g}{4}(r_a + r_b\cos\alpha)\\
&\quad + K_f L_i\cos(\phi_a + \Omega t),\\
\Omega &= \omega - \frac{r_b}{4 r_a} g\sin\alpha - \frac{K_f L_i}{r_a}\sin(\phi_a + \Omega t),\\
0 &= \gamma r_b(A - r_b) + \frac{g}{4}(r_a\cos\alpha + r_b),\\
\Omega &= \omega + \frac{r_a}{4 r_b} g\sin\alpha.
\end{aligned} \tag{13}$$

$L_c = L_i\cos(\phi_a + \Omega t)$ and $L_s = L_i\sin(\phi_a + \Omega t)$ are related to the light–dark schemes, and the schemes can be expressed by piecewise functions. Therefore,

the values of L_c and L_s for the rectangular scheme are calculated by piecewise integration as follows

$$\begin{aligned} L_c &= \frac{\int_0^{\frac{T}{2}} \cos(\phi_a + \Omega t)\, dt}{T} = -\frac{\sin\phi_a}{\pi}, \\ L_s &= \frac{\int_0^{\frac{T}{2}} \sin(\phi_a + \Omega t)\, dt}{T} = \frac{\cos\phi_a}{\pi}. \end{aligned} \tag{14}$$

The values of L_c and L_s for the sinusoidal scheme are calculated by piecewise integration as follows

$$\begin{aligned} L_c &= \frac{\int_0^{T} \frac{\sin(\Omega t)+1}{2} \cos(\phi_a + \Omega t)\, dt}{T} = -\frac{\sin\phi_a}{4}, \\ L_s &= \frac{\int_0^{T} \frac{\sin(\Omega t)+1}{2} \sin(\phi_a + \Omega t)\, dt}{T} = \frac{\cos\phi_a}{4}. \end{aligned} \tag{15}$$

The calculation formulas of other schemes are not displayed below, and the values of L_c and L_s are directly shown in Table 1.

When Ω reaches the maximum value, LLE = $\frac{2\pi}{\Omega_{max}}$ is obtained. Without losing generality, we will compare the values of the LLE for the five light–dark schemes under the conditions of $g \ll K_f$ and $g \gg K_f$.

When $g \ll K_f$, it can be obtained that $\sin\alpha \approx 1$ and $\cos\phi_a \approx 0$ according to Ref. [35]. Therefore, Eq. (13) can be simplified as

$$\begin{aligned} 0 &= \gamma r_a(A - r_a) + \frac{g}{4} r_a + K_f L_i \cos(\phi_a + \Omega t), \\ \Omega_{max} &= \omega - \frac{r_b}{4r_a} g - \frac{K_f L_i}{r_a} \sin(\phi_a + \Omega t), \\ 0 &= \gamma r_b(A - r_b) + \frac{g}{4} r_b, \\ \Omega_{max} &= \omega + \frac{r_a}{4r_b} g. \end{aligned} \tag{16}$$

According to the first and the third equations of Eq. (16), we obtain

$$\begin{aligned} r_a &= A + \frac{g}{4\gamma} + \frac{4K_f}{4A\gamma + g} L_i \cos(\phi_a + \Omega t), \\ r_b &= A + \frac{g}{4\gamma}. \end{aligned} \tag{17}$$

According to the second and the fourth equations of Eq. (16), we obtain

$$\begin{aligned} \Omega_{max} = \omega + \frac{g}{8}\left(\frac{r_a}{r_b} - \frac{r_b}{r_a}\right) \\ - \frac{K_f}{2r_a} L_i \sin(\phi_a + \Omega t). \end{aligned} \tag{18}$$

Due to $\cos\phi_a \approx 0$, we can obtain $\sin\phi_a \approx -1$. Equation (18) can be simplified as

$$\Omega_{max} = \omega + \frac{g}{8}\left(\frac{r_a}{r_b} - \frac{r_b}{r_a}\right). \tag{19}$$

Table 1 The values of L_c and L_s for the five light–dark schemes

	LD	TRA	SINE	TRI	SAW
L_c	$\frac{-\sin\phi_a}{\pi}$	$\frac{-12\cos\frac{5\pi}{12}\sin\phi_a}{\pi^2}$	$\frac{-\sin\phi_a}{4}$	$\frac{-2\sin\phi_a}{\pi^2}$	$\frac{-\sin\phi_a}{2\pi}$
L_s	$\frac{\cos\phi_a}{\pi}$	$\frac{12\cos\frac{5\pi}{12}\cos\phi_a}{\pi^2}$	$\frac{\cos\phi_a}{4}$	$\frac{2\cos\phi_a}{\pi^2}$	$\frac{\cos\phi_a}{2\pi}$

According to the values of L_c for the five light–dark schemes in Table 1 and $\sin\phi_a \approx -1$, we can obtain $\frac{1}{\pi} > \frac{12\cos\frac{5\pi}{12}}{\pi^2} > \frac{1}{4} > \frac{2}{\pi^2} > \frac{1}{2\pi}$. From Eq. (17), we obtain $r_a > r_c$, and r_a(rectangular) > r_a(trapezoidal) > r_a(sinusoidal) > r_a(triangular) > r_a(sawtooth). The larger value of r_a is, the larger value of $\frac{r_a}{r_b} - \frac{r_b}{r_a}$ is. From Eq. (19), we obtain Ω_{max}(rectangular) > Ω_{max}(trapezoidal) > Ω_{max}(sinusoidal) > Ω_{max}(triangular) > Ω_{max}(sawtooth), i.e., LLE(rectangular) < LLE(trapezoidal) < LLE(sinusoidal) < LLE(triangular) < LLE(sawtooth), which confirms the results in Fig. 6.

When $g > K_f$, it can be known $\sin\alpha \approx \alpha$ and $\cos\phi_a \approx -1$ from Ref. [35]. Therefore, Eq. (13) can be simplified as

$$\begin{aligned} 0 &= \gamma r_a(A - r_a) + \frac{g}{4}(r_a + r_b) \\ &\quad + K_f L_i \cos(\phi_a + \Omega t), \\ \Omega &= \omega - \frac{r_b}{4r_a} g\alpha - \frac{K_f L_i}{r_a} \sin(\phi_a + \Omega t), \\ 0 &= \gamma r_b(A - r_b) + \frac{g}{4}(r_a + r_b), \\ \Omega &= \omega + \frac{r_a}{4r_b} g\alpha. \end{aligned} \tag{20}$$

Due to $\cos\phi_a \approx -1$, $L_c \approx 0$ can be obtained. From the first and the third equations of Eq. (20), we obtain

$$r_a \approx r_b \approx A + \frac{g}{2\gamma}. \tag{21}$$

From the second and the fourth equations of Eq. (20), we obtain

$$\Omega_{max} = \omega - \frac{K_f L_i}{2r_a} \sin(\phi_a + \Omega t). \tag{22}$$

Due to $\cos\phi_a \approx -1$, we can obtain $\sin\phi_a \approx 0$. According to the values of L_s for the five light–dark schemes in Table 1, we can obtain $-\frac{1}{\pi} < -\frac{2\sqrt{2}}{\pi^2} < -\frac{1}{4} < -\frac{2}{\pi^2} < -\frac{1}{2\pi}$. From Eq. (22), we can obtain Ω_{max}(rectangular) > Ω_{max}(trapezoidal) > Ω_{max}(sinusoidalE) > Ω_{max}(triangular) > Ω_{max}

Table 2 The values of L_c and L_s for the 12:12 h rectangular scheme and different sinusoidal schemes

	LD	SINE I	SINE II	SINE
L_c	$\frac{-\sin\phi_a}{\pi}$	$\frac{-\pi\sin\phi_a}{6}$	$\frac{-\sin\phi_a}{4}$	$\frac{-\sin\phi_a}{4}$
L_s	$\frac{\cos\phi_a}{\pi}$	$\frac{\pi\cos\phi_a}{6}$	$\frac{\cos\phi_a}{4}$	$\frac{\cos\phi_a}{4}$

Table 3 The values of L_c and L_s for the rectangular schemes

	LD	LD I	LD II	LD III
L_c	$\frac{-\sin\phi_a}{\pi}$	$\frac{-3\sin\phi_a}{4\pi}$	$\frac{-4\sin\phi_a}{3\pi}$	$\frac{-9\sin\phi_a}{16\pi}$
L_s	$\frac{\cos\phi_a}{\pi}$	$\frac{3\cos\phi_a}{4\pi}$	$\frac{4\cos\phi_a}{3\pi}$	$\frac{9\cos\phi_a}{16\pi}$

Table 4 The values of L_c and L_s for the sinusoidal schemes

	SINE II	SINE III	SINE IV	SINE V
L_c	$\frac{-\sin\phi_a}{4}$	$\frac{-4\sqrt{3}\sin\phi_a}{7\pi}$	$\frac{-\sin\phi_a}{3}$	$\frac{-3\sqrt{3}\sin\phi_a}{7\pi}$
L_s	$\frac{\cos\phi_a}{4}$	$\frac{4\sqrt{3}\cos\phi_a}{7\pi}$	$\frac{\cos\phi_a}{3}$	$\frac{3\sqrt{3}\cos\phi_a}{7\pi}$

(sawtooth), i.e., LLE(rectangular) < LLE(trapezoidal) < LLE(sinusoidal) < LLE(triangular) < LLE(sawtooth), which confirms the results in Fig. 6.

Therefore, the LLE of the five light–dark schemes are closely related to the values of L_c and L_s. With the increase of $|L_c|$ and $|L_s|$, the LLE decreases, i.e., the entrainment range increases.

Similarly, the values of L_c and L_s in Figs. 2, 3 and 4 are shown in Tables 2, 3 and 4, respectively. The theoretical analysis results in Tables 2, 3 and 4 are consistent with the numerical simulation results of Figs. 8, 9 and 10.

Finally, we analyze the relationship between the entrainment range and the photoperiod of the rectangular scheme and the sinusoidal scheme. When the photoperiod of the rectangular scheme is m, the values of L_c and L_s are shown in Eq. (23).

$$\begin{aligned} L_c &= \frac{\int_0^{\frac{mT}{24}} \cos(\phi_a + \Omega t)\, dt}{T} \\ &= -\frac{1}{\pi}\left(\sin\frac{m\pi}{24}\right)^2 \sin\phi_a, \\ L_s &= \frac{\int_0^{\frac{mT}{24}} \sin(\phi_a + \Omega t)\, dt}{T} \\ &= \frac{1}{\pi}\left(\sin\frac{m\pi}{24}\right)^2 \cos\phi_a. \end{aligned} \tag{23}$$

Let $f(m) = \frac{1}{\pi}(\sin\frac{m\pi}{24})^2$, we can obtain the derivative of $f(m)$ in Eq. (24).

$$f'(m) = \frac{1}{12}\sin\frac{m\pi}{24}\cos\frac{m\pi}{24}. \tag{24}$$

When $f'(m) = 0$, we obtain $m = 0, 12, 24$. When $m = 12$, the maximum $|L_c|$ and $|L_s|$, i.e., the maximum entrainment range, can be obtained, and the result is consistent with Fig. 11.

When the photoperiod of the sinusoidal scheme is n, the values of L_c and L_s are shown in Eq. (25).

$$\begin{aligned} L_c &= \frac{\int_0^{\frac{nT}{24}} \sin(\frac{24\pi}{nT}t)\cos(\phi_a + \Omega t)\, dt}{T} \\ &= \frac{n}{2\pi}\left(\frac{1}{24+2n} \right. \\ &\quad \left. + \frac{1}{2n-24}\right)\sin\frac{n\pi}{12}\sin\phi_a, \\ L_s &= \frac{\int_0^{\frac{nT}{24}} \sin(\frac{24\pi}{nT}t)\sin(\phi_a + \Omega t)\, dt}{T} \\ &= -\frac{n}{2\pi}\left(\frac{1}{24+2n} \right. \\ &\quad \left. + \frac{1}{2n-24}\right)\sin\frac{n\pi}{12}\cos\phi_a. \end{aligned} \tag{25}$$

Let $g(n) = -\frac{n}{2\pi}(\frac{1}{24+2n} + \frac{1}{2n-24})\sin\frac{n\pi}{12}$, we can obtain the derivative of $g(n)$ in Eq. (26).

$$\begin{aligned} g'(n) = &-\frac{1}{2\pi}\left(\frac{1}{24+2n} + \frac{1}{2n-24}\right)\sin\frac{n\pi}{12} \\ &- \frac{n}{2\pi}\left[\frac{-2}{(24+2n)^2} + \frac{-2}{(2n-24)^2}\right]\sin\frac{n\pi}{12} \\ &- \frac{n}{24}\left(\frac{1}{24+2n} + \frac{1}{2n-24}\right)\cos\frac{n\pi}{12}. \end{aligned} \tag{26}$$

When $g'(n) = 0$, we obtain $m = 0, 16$. When $m = 16$, the maximum $|L_c|$ and $|L_s|$, i.e., the maximum entrainment range, can be obtained, and the result is consistent with Fig. 11.

5 Discussion and conclusion

In most experimental studies of circadian rhythms, a rectangular scheme was applied, meaning a sudden transition from light to dark and vice versa. In this paper, we theoretically analyzed the influences of the five light–dark schemes on the entrainment characteristics of the SCN, using a Poincaré model [33]. We

showed that more light during the day time lead to a larger range of entrainment, irrespective of light in the night period. Moreover, with the same amount of light exposure during the day, a higher maximum light intensity during the day also lead to a larger range of entrainment. Moreover, we found that the ability to entrain to different light–dark periods changes with seasonal adaptation. Depending on the light–dark scheme, the entrainment ability was altered when different photoperiods were applied. For the rectangular scheme, the maximum entrainment ability was reached when the photoperiod was 12 h in one 24-h cycle. However, for the sinusoidal scheme, the maximum entrainment ability was reached when the photoperiod was 16 h in one 24-h cycle. This should be considered when designing experiments and choosing a light–dark scheme.

Without loss of generality, we also considered the Goodwin model and presented the results in the supplementary materials (figure R1) [32]. The results are qualitatively consistent with the results in the paper. For simplicity, we considered the all-to-all connected network in this paper. However, in the SCN network, the connections between neuronal oscillators are not all-to-all connected. We also considered a Barabási-Albert (BA) scale free network and an Erdös-Rényi (ER) random network in the supplementary materials (figure R2 and R3) [41]. The results are qualitatively consistent with the results in the paper.

To sum up, the light–dark scheme which the SCN was exposed to has a large impact on the ability of the SCN to entrain to different periods of the light–dark cycle. A larger entrainment ability was reached when (i) it was exposed to more light during the day, (ii) the maximum light intensity during the light period was higher, and (iii) this depended on different photoperiods. However, this last option differs between the different light–dark schemes.

How much of the natural light–dark cycle an animal actually perceives is still not entirely clear. De Coursey, et al., found that nocturnal animals saw light for only a brief amount of time (0.4–3.5% of the photoperiod) mainly at dusk [42]. Hut, et al., investigated diurnal animals and found that these animals generated their own patterns of exposure to light within the natural light–dark cycle, by emerging from their burrows a few hours after dawn and returning to their burrows a few hours before dusk [43]. This showed that the light exposure was obviously different between nocturnal and diurnal animals. This difference may have a great impact on the results shown in this paper. Here we assumed that animals perceived the light throughout the cycle. If more information on the actual light that is perceived by different species becomes available, this study should get a follow-up to incorporate these results.

In addition to the difference of external light intensity, organisms also have different sensitivity to light, which affects the flexibility of circadian rhythms [7, 16, 18, 19, 44, 45]. Therefore, the differences between species will also change the results presented here. However, we believe that the general message provided in our study provides a solid basis that can be used in future experimental studies.

This study is relevant to health and disease. A larger ability to entrain leads to a faster recovery from, for example, jet lag or night shift work. Individuals who are more sensitive to light have better adaptability to jet lag. Because women and the elderly are less sensitive to light information than men, they are more vulnerable to jet lag and are not able to recover easily [46–50]. Increasing the range of entrainment, and thus the flexibility of the SCN clock, by providing more light during the day, with higher light intensity, may help these people recover more quickly from detrimental effects of jet lag. Moreover, long-term exposure to light at night will also destroy the circadian rhythm of organisms, resulting in physiological and behavioral changes in, amongst others, nocturnal rodents [51]. Therefore, appropriate light intensity and light duration are very important for diurnal and nocturnal animals, which can not only reduce the occurrence of related diseases, but also enhance their adaptability to external environmental changes [4]. In conclusion, we believe that we offer a well-defined framework that identifies differences in light–dark schemes, and show the importance of well-chosen light–dark schemes for different purposes.

Acknowledgements The work is supported by the National Natural Science Foundation of China under Grant Nos. 12275179 and 11875042, and Natural Science Foundation of Shanghai (Grant No. 21ZR1443900). Jos Rohling was supported by the European Research Council Advanced Grant in the Diurnal Helath grant No. 854513 (ERC-2018-ADC).

Data availability The authors declare that the manuscript has no associated data

Declarations

Conflict of interest The authors declare that they have no conflict of interest.

References

1. Schmal, C., Herzel, H., Myung, J.: Clocks in the wild: entrainment to natural light. Front. Physiol. **11**, 272 (2020)
2. Wheeler, D.A., Hamblen-Coyle, M.J., Dushay, M.S., Hall, J.C.: Behavior in light-dark cycles of Drosophila mutants that are arrhythmic, blind, or both. J. Biol. Rhythms **8**(1), 67–94 (1993)
3. Usui, S., Takahashi, Y., Okazaki, T.: Range of entrainment of rat circadian rhythms to sinusoidal light-intensity cycles. Am. J. Physiol.-Regul. Integr. Comp. Physiol. **278**(5), R1148–R1156 (2000)
4. Madahi, P.G., Ivan, O., Adriana, B., Diana, O., Carolina, E.: Constant light during lactation programs circadian and metabolic systems. Chronobiol. Int. **35**(8), 1153–1167 (2018)
5. Ananthasubramaniam, B., Schmal, C., Herzel, H.: Amplitude effects allow short jet lags and large seasonal phase shifts in minimal clock models. J. Mol. Biol. **432**(12), 3722–3737 (2020)
6. Abraham, U., Granada, A.E., Westermark, P.O., Heine, M., Kramer, A., Herzel, H.: Coupling governs entrainment range of circadian clocks. Mol. Syst. Biol. **6**, 438 (2010)
7. Meijer, J.H., Schwartz, W.J.: In search of the pathways for light-induced pacemaker resetting in the suprachiasmatic nucleus. J. Biol. Rhythms **18**(3), 235–249 (2003)
8. Refinetti, R.: Circadian Physiology. CRC Press, Boca Raton (2006)
9. Campuzano, A., Vilaplana, J., Cambras, T., DiezNoguera, A.: Dissociation of the rat motor activity rhythm under T cycles shorter than 24 hours. Physiol. Behav. **63**(2), 171–176 (1998)
10. Meijer, J.H., Rusak, B., Harrington, M.E.: Photically responsive neurons in the hypothalamus of a diurnal ground squirrel. Brain Res. **501**(2), 315–23 (1989)
11. Reppert, S.M., Weaver, D.R.: Coordination of circadian timing in mammals. Nature **418**(6901), 935–941 (2002)
12. Moore, R.Y., Speh, J.C., Leak, R.K.: Suprachiasmatic nucleus organization. Cell Tissue Res. **309**(1), 89–98 (2002)
13. Michel, S., Meijer, J.H.: From clock to functional pacemaker. Eur. J. Neurosci. **51**(1), 482–493 (2020)
14. Sujino, M., Koinuma, S., Minami, Y., Shigeyoshi, Y.: Heavy water lengthens the molecular circadian clock period in the suprachiasmatic nucleus of mice in vitro. J. Biol. Rhythms **36**(4), 410–418 (2021)
15. Smyllie, N.J., Bagnall, J., Koch, A.A., Niranjan, D., Polidarova, L., Chesham, J.E., Chin, J.W., Partch, C.L., Loudon, A.S.I., Hastings, M.H.: Cryptochrome proteins regulate the circadian intracellular behavior and localization of PER2 in mouse suprachiasmatic nucleus neurons. Proc. Natl. Acad. Sci. U. S. A. **119**(4), e2113845119 (2022)
16. Lee, H.S., Nelms, J.L., Nguyen, M., Silver, R., Lehman, M.N.: The eye is necessary for a circadian rhythm in the suprachiasmatic nucleus. Nat. Neurosci. **6**(2), 111–112 (2003)
17. VanderLeest, H.T., Rohling, J.H.T., Michel, S., Meijer, J.H.: Phase shifting capacity of the circadian pacemaker determined by the SCN neuronal network organization. Plos One **4**(3), e4976 (2009)
18. Rohling, J.H.T., Vanderleest, H.T., Michel, S., Vansteensel, M.J., Meijer, J.H.: Phase resetting of the Mammalian circadian clock relies on a rapid shift of a small population of pacemaker neurons. Plos One **6**(9), e25437 (2011)
19. Gu, C.G., Liu, Z.H., Schwartz, W.J., Indic, P.: Photic desynchronization of two subgroups of circadian oscillators in a network model of the suprachiasmatic nucleus with dispersed coupling strengths. Plos One **7**(5), e36900 (2012)
20. Li, Y.N., Androulakis, I.P.: Light entrainment of the SCN circadian clock and implications for personalized alterations of corticosterone rhythms in shift work and jet lag. Sci. Rep. **11**(1), 17929 (2021)
21. Hattar, S., Liao, H.W., Takao, M., Berson, D.M., Yau, K.W.: Melanopsin-containing retinal. Ganglion cells: architecture, projections, and intrinsic photosensitivity. Science **295**(5557), 1065–1070 (2002)
22. Panda, S., Nayak, S.K., Campo, B., Walker, J.R., Hogenesch, J.B., Jegla, T.: Illumination of the melanopsin signaling pathway. Science **307**(5709), 600–604 (2005)
23. Mieda, M., Ono, D., Hasegawa, E., Okamoto, H., Honma, K., Honma, S., Sakurai, T.: Cellular clocks in AVP neurons of the SCN Are critical for interneuronal coupling regulating circadian behavior rhythm. Neuron **85**(5), 1103–1116 (2015)
24. Breitenbach, T., Helfrich-Forster, C., Dandekar, T.: An effective model of endogenous clocks and external stimuli determining circadian rhythms. Sci. Rep. **11**(1), 16165 (2021)
25. Pikovsky, A., Rosenblum, M., Kurths, J.: Synchronization: A Universal Concept in Nonlinear Science. Cambridge University Press, New York (2001)
26. Boulos, Z., Macchi, M., Terman, M.: Twilight transitions promote circadian entrainment to lengthening light-dark cycles. Am. J. Physiol. **271**(3), R813-8 (1996)
27. Boulos, Z., Macchi, M.M., Terman, M.: Twilights widen the range of photic entrainment in hamsters. J. Biol. Rhythms **17**(4), 353–363 (2002)
28. Boulos, Z., Macchi, M.M.: Season- and latitude-dependent effects of simulated twilights on circadian entrainment. J. Biol. Rhythms **20**(2), 132–144 (2005)
29. Comas, M., Hut, R.A.: Twilight and photoperiod affect behavioral entrainment in the house mouse (Mus musculus). J. Biol. Rhythms **24**(5), 403–412 (2009)
30. Gu, C.G., Xu, J.S., Liu, Z.H., Rohling, J.H.T.: Entrainment range of nonidentical circadian oscillators by a light-dark cycle. Phys. Rev. E. **88**(2), 022702 (2013)
31. Granada, A.E., Bordyugov, G., Kramer, A., Herzel, H.: Human chronotypes from a theoretical perspective. Plos One **8**(3), e59464 (2013)
32. Gu, C.G., Ramkisoensing, A., Liu, Z.H., Meijer, J.H., Rohling, J.H.T.: The proportion of light-responsive neurons determines the limit cycle properties of the suprachiasmatic nucleus. J. Biol. Rhythms **29**(1), 16–27 (2014)
33. Gu, C.G., Yang, H.J.: The asymmetry of the entrainment range induced by the difference in intrinsic frequencies between two subgroups within the suprachiasmatic nucleus. Chaos **27**(6), 063115 (2017)
34. Bordyugov, G., Abraham, U., Granada, A., Rose, P., Imkeller, K., Kramer, A., Herzel, H.: Tuning the phase of circadian entrainment. J. Royal Soc. Interface **12**(108), 20150282 (2015)

35. Zheng, W.X., Gu, C.G., Yang, H.J., Rohling, J.H.T.: Motif structure for the four subgroups within the suprachiasmatic nuclei affects its entrainment ability. Phys. Rev. E. **105**(1), 014314 (2022)
36. Tokuda, I.T., Ono, D., Ananthasubramaniam, B., Honma, S., Honma, K., Herzel, H.: Coupling controls the synchrony of clock cells in development and knockouts. Biophys. J. **109**(10), 2159–2170 (2015)
37. Gu, C.G., Tang, M., Rohling, J.H.T., Yang, H.J.: The effects of non-self-sustained oscillators on the en-trainment ability of the suprachiasmatic nucleus. Sci. Rep. **6**, 37661 (2016)
38. Gu, C.G., Yang, H.J., Wang, M.: Dispersion of the intrinsic neuronal periods affects the relationship of the entrainment range to the coupling strength in the suprachiasmatic nucleus. Phys. Rev. E. **96**(5), 052207 (2017)
39. Gu, C.G., Rohling, J.H.T., Liang, X.M., Yang, H.J.: Impact of dispersed coupling strength on the free running periods of circadian rhythms. Phys. Rev. E. **93**(3), 032414 (2016)
40. Gu, C.G., Yang, H.J., Ruan, Z.Y.: Entrainment range of the suprachiasmatic nucleus affected by the difference in the neuronal amplitudes between the light-sensitive and light-insensitive regions. Phys. Rev. E. **95**(4), 042409 (2017)
41. Gu, C.G., Yang, H.J.: The circadian rhythm induced by the heterogeneous network structure of the suprachiasmatic nucleus. Chaos **26**(5), 053112 (2016)
42. DeCoursey, P.J.: Light-sampling behavior in photoentrainment of a rodent circadian rhythm. J. Comp. Physiol. A-Neuroethol. Sens. Neural Behav. Physiol. **159**(2), 161–9 (1986)
43. Hut, R.A., van Oort, B.E.H., Daan, S.: Natural entrainment without dawn and dusk: the case of the European ground squirrel (Spermophilus citellus). J. Biol. Rhythms **14**(4), 290–299 (1999)
44. Schwartz, M.D., Wotus, C., Liu, T.C., Friesen, W.O., Borjigin, J., Oda, G.A., de la Iglesia, H.O.: Dissociation of circadian and light inhibition of melatonin release through forced desynchronization in the rat. Proc. Natl. Acad. Sci. U. S. A. **106**(41), 17540–17545 (2009)
45. Gu, C.G., Yang, H.J., Rohling, J.H.T.: Dissociation between two subgroups of the suprachiasmatic nucleus affected by the number of damped oscillated neurons. Phys. Rev. E. **95**(3), 032302 (2017)
46. Kolla, B.P., Auger, R.R.: Jet lag and shift work sleep disorders: how to help reset the internal clock. Cleveland Clin. J. Med. **78**(10), 675–684 (2011)
47. Diaz-Morales, J.F., Escribano, C.: Social jetlag, academic achievement and cognitive performance: understanding gender/sex differences. Chronobiol. Int. **32**(6), 822–831 (2015)
48. Daneault, V., Dumont, M., Masse, E., Vandewalle, G., Carrier, J.: Light-sensitive brain pathways and aging. J. Physiol. Anthropol. **35**, 9 (2016)
49. Santhi, N., Lazar, A.S., McCabe, P.J., Lo, J.C., Groeger, J.A., Dijk, D.J.: Sex differences in the circadian regulation of sleep and waking cognition in humans. Proc. Natl. Acad. Sci. U. S. A. **113**(19), E2730–E2739 (2016)
50. Chellappa, S.L., Steiner, R., Oelhafen, P., Cajochen, C.: Sex differences in light sensitivity impact on brightness perception, vigilant attention and sleep in humans. Sci. Rep. **7**, 14215 (2017)
51. Fonken, L.K., Nelson, R.J.: The effects of light at night on circadian clocks and metabolism. Endocr. Rev. **35**(4), 648–670 (2014)